Available online at www.sciencedirect.com
ScienceDirect
Mathematics and Computers in Simulation 204 (2023) 216–229
MATHEMATICS AND COMPUTERS IN SIMULATION
www.elsevier.com/locate/matcom

Original articles

Direct WENO scheme for dispersion-type equations☆

Muyassar Ahmat[a,b], Jianxian Qiu[c,*]

[a] School of Mathematical Sciences, Xiamen University, Xiamen, Fujian 361005, PR China
[b] College of Mathematics and Systems Science, Xinjiang University, Urumqi, Xinjiang 830046, PR China
[c] School of Mathematical Sciences and Fujian Provincial Key Laboratory of Mathematical Modeling and High-Performance Scientific Computing, Xiamen University, Xiamen, Fujian 361005, PR China

Received 21 October 2021; received in revised form 5 June 2022; accepted 18 August 2022
Available online 27 August 2022

Abstract

In this paper, we present a weighted essentially non-oscillatory (WENO) scheme for dispersive equations which may generate physical high-frequency oscillation in the non-smooth interface. The third derivative term is approximated directly by a conservative flux difference. A finite-difference WENO scheme of fifth-order is constructed for the discretization of spatial differentiation. The wave behavior of linear and nonlinear dispersion equations is simulated by using the proposed scheme in space direction and the third-order TVD Runge–Kutta method in the time direction. Numerical examples demonstrate the accuracy and good performance of the proposed scheme.

Keywords: Dispersive equation; High-frequency oscillation; WENO scheme; TVD Runge–Kutta method

1. Introduction

Weighted essentially non-oscillatory (WENO) schemes are generally used to approximate hyperbolic conservation laws and the convection terms in convection-dominated partial differential equations (PDEs). After the first introduction of the third-order accurate finite volume WENO scheme in 1994 by Liu, Osher, and Chan [14] in one space dimension, a general framework for designing arbitrary order accurate finite difference WENO schemes was provided by Jiang and Shu [11] in 1996. Various types of highly effective conservative finite volume and conservative finite difference WENO schemes were further developed to solve hyperbolic conservation laws since then by many researchers [4,7,8,12,15,24,25].

Since the last decade, researchers have also paid attention to the discretization of the second derivative by the WENO method. Consequently, the finite difference WENO technique was presented originally for the nonlinear degenerate parabolic equations which may contain discontinuous solutions in [16]. A new finite difference WENO procedure was given by using optimum polynomial in the stencil in [2]. Both explicit and implicit finite volume WENO schemes were developed on non-uniform computational meshes in [3]. An efficient sixth-order finite difference WENO scheme was obtained with a new type of nonlinear weight by Rathan [20]. High order finite

☆ The research is partly supported by National Natural Science Foundation of China grant 12071392.
* Corresponding author.
E-mail addresses: muyassar@stu.xmu.edu.cn (M. Ahmat), jxqiu@xmu.edu.cn (J. Qiu).

https://doi.org/10.1016/j.matcom.2022.08.010

difference multi-resolution WENO method for the second derivative was constructed in [10]. A six-order finite difference WENO method was constructed based on Legendre orthogonal monic polynomial in [1].

In this paper, we design a direct WENO scheme for dispersive equations in which the third derivative is included. The solution of dispersive equations may have smooth, high-frequency oscillation or shock wave behavior, depended on the non-linearity and smoothness of the function. Our main focus in this paper is the prototype equation of the form in the following:

$$u_t + f(u)_x + g(u)_{xxx} = 0. \tag{1.1}$$

For such type of dispersion-dominated equations, we here describe the Rosenau–Hyman equation, which also called $K(n, m)$ equation: $u_t + (u^n)_x + (u^m)_{xxx} = 0$, specifically. For certain values of n and m, the Rosenau–Hyman equation has compactly supported solitary wave solutions. These structures, the so-called compactons, have several things in common with soliton solutions of the Korteweg–de Vries (KdV) equation. For example, a single compacton moves with a velocity that is proportional to its amplitude. Several compactons with different velocities move and collide, and experience nonlinear interactions, resulting in phase shifts. In addition, one general initial data can be decomposed into a series of compactons. The compacton is continuous at the endpoints of its compact support, but the first derivative of the compacton at the endpoints is discontinuous. Physical oscillations occur near these points and become more pronounced as the degree of nonlinearity increases.

The numerical solution of the Rosenau–Hyman equation is a challenging problem due to the co-existence of dispersion effect and nonlinearity. The widely used numerical method is the pseudo-spectral method in space [5,21]. These methods require the use of high-pass filter for artificial dissipation (hyperviscosity), and also retain the positiveness of the solution, but the sign may change after the compacton collision. The finite difference method with Padé approximation [19], the local discontinuous Galerkin method [13], the second-order finite difference method [9] and the line method [22] based on adaptive mesh refinement have also been successfully applied.

The dispersive wave Eq. (1.1) has features that are similar to those of hyperbolic conservation law, such as the possible existence of sharp fronts and the finite speed of propagation of wavefronts. Therefore, it is reasonable to generalize the numerical techniques for solving hyperbolic conservation laws, such as the WENO technique, to solve (1.1). This would involve a careful adaptation of the WENO procedure to ensure the conservation, accuracy, and non-oscillatory performance. In this paper, the direct WENO scheme for the third derivative is introduced in detail. In Section 2, we present the high order direct WENO approximation procedure, also the specific description and analysis of fifth-order WENO approximation. In Section 3, the numerical method in the time direction and corresponding CFL restriction is analyzed. The accuracy and non-oscillatory performance of the fifth-order direct WENO scheme for the third derivative are provided by numerical examples in Section 4. In Section 5, we give brief concluding remarks.

2. Direct finite difference WENO scheme for dispersive equations

We derive a direct finite difference WENO scheme to the third derivative in conservation form. Assume the uniform mesh is distributed as follows:

$$\begin{aligned} x \in [x_l, x_r], \quad x_j = x_l + (j-1)\Delta x, \quad j = 1:N, \quad x_1 = x_l, \quad x_N = x_r, \\ I_j = [x_{j-\frac{1}{2}}, x_{j+\frac{1}{2}}], \quad x_{j+\frac{1}{2}} = \frac{x_{j+1} + x_j}{2}. \end{aligned} \tag{2.1}$$

where Δx is the spatial step size. u_j is defined as a nodal point value $u(x_j, t)$.

We are constructing the following conservative finite difference scheme for (1.1) of the form:

$$\frac{du_j}{dt} = -\frac{\hat{F}_{j+\frac{1}{2}} - \hat{F}_{j-\frac{1}{2}}}{\Delta x} - \frac{\hat{G}_{j+\frac{1}{2}} - \hat{G}_{j-\frac{1}{2}}}{\Delta x}. \tag{2.2}$$

where $\hat{F}$ and $\hat{G}$ are the numerical flux for convection and dispersion, respectively. For the convection flux, we require it is consistent with the physical flux $\hat{F}(u, \ldots, u) = f(u)$, also is Lipschitz continuous with respect to all its arguments.

For the treatment of the convection term is a well researched topic in conservation laws, the readers can refer to [11] for the detailed construction procedure. At the end of this section, we give a brief (Remark 3) for the specific calculation method of the convection term in practice.

We will focus on the dispersion term and present a kth order accurate conservative finite difference scheme as:

$$\frac{\hat{G}_{j+\frac{1}{2}} - \hat{G}_{j-\frac{1}{2}}}{\Delta x} \approx g(u)_{xxx}|_{x=x_j} + O(\Delta x^k). \tag{2.3}$$

where $\hat{G}_{j+\frac{1}{2}}$ is a numerical dispersion flux at the cell boundary $x_{j+\frac{1}{2}}$.

We define function $p(x)$ implicitly, such that:

$$g(u) = \frac{1}{\Delta x^3}\int_{x-\frac{\Delta x}{2}}^{x+\frac{\Delta x}{2}}\int_{\eta-\frac{\Delta x}{2}}^{\eta+\frac{\Delta x}{2}}\int_{\xi-\frac{\Delta x}{2}}^{\xi+\frac{\Delta x}{2}} p(\theta)d\theta d\xi d\eta, \tag{2.4}$$

then by triple derivation, we have

$$g(u)_{xxx} = \frac{p(x+\frac{3}{2}\Delta x) - 3p(x+\frac{1}{2}\Delta x) + 3p(x-\frac{1}{2}\Delta x) - p(x-\frac{3}{2}\Delta x)}{\Delta x^3}. \tag{2.5}$$

We define function $G(x)$, such that

$$G(x) = \frac{p(x+\Delta x) - 2p(x) + p(x-\Delta x)}{\Delta x^2}, \tag{2.6}$$

then we have

$$g(u)_{xxx}|_{x=x_j} = \frac{G(x_{j+\frac{1}{2}}) - G(x_{j-\frac{1}{2}})}{\Delta x}. \tag{2.7}$$

If we have numerical flux $\hat{G}_{j+\frac{1}{2}}$ which is an approximation to $G(x_{j+\frac{1}{2}})$ up to kth order, then we have Eq. (2.3).

For stability, it is similar to the reconstruction procedure for numerical fluxes for convection terms, we split $g(u)$ into two parts, that is $g(u) = g^+(u) + g^-(u)$ with $\frac{\partial g^+(u)}{\partial u} \geq 0$ and $\frac{\partial g^-(u)}{\partial u} \leq 0$, and $G^+(x)$ and $G^-(x)$ are defined by (2.6) according to $g^+(u)$ and $g^-(u)$, respectively. We would like to reconstruct numerical fluxes $\hat{G}^+_{j+\frac{1}{2}}$ and $\hat{G}^-_{j+\frac{1}{2}}$ to approximate $G^+(x_{j+\frac{1}{2}})$ and $G^-(x_{j+\frac{1}{2}})$ up to k order, respectively. Finally, we define numerical fluxes $\hat{G}_{j+\frac{1}{2}}$ as:

$$\hat{G}_{j+\frac{1}{2}} = \hat{G}^+_{j+\frac{1}{2}} + \hat{G}^-_{j+\frac{1}{2}},$$

and $\hat{G}_{j+\frac{1}{2}}$ is an approximation to $G(x_{j+\frac{1}{2}})$ up to k order.

Now we would like to describe the reconstruction procedure for $\hat{G}^+_{j+\frac{1}{2}}$, and procedure for $\hat{G}^-_{j+\frac{1}{2}}$ is mirror symmetric respect to $x_{j+\frac{1}{2}}$.

Step 1: We choose a big stencil, $S = [x_{j-r}, \ldots, x_{j+r+2}]$, resulting in a scheme with order of accuracy $k = 2r+1$. In this stencil, a polynomial $\rho(x)$ of degree $2r+2$ based on node information can be obtained, which is used to approximate $p(x)$ and satisfies:

$$\frac{1}{\Delta x^3}\int_{x_m-\frac{\Delta x}{2}}^{x_m+\frac{\Delta x}{2}}\int_{\eta-\frac{\Delta x}{2}}^{\eta+\frac{\Delta x}{2}}\int_{\xi-\frac{\Delta x}{2}}^{\xi+\frac{\Delta x}{2}} \rho(\theta)d\theta d\xi d\eta = g^+_m, \quad m = j-r, \ldots, j+r+2. \tag{2.8}$$

Now we can obtain polynomial approximation $h(x)$ of $G(x)$ by (2.6). If the fifth-order approximation is taken into specification, which in the case of $r = 2$, the explicit polynomial expression $h(x)$ of degree at most four in this stencil:

$$\begin{aligned} h(x) = &\frac{1}{\Delta x^2}\Big[\ \frac{1}{1920}\Big(-4725g^+_j + 2140g^+_{j+1} + 315g^+_{j+2} - 222g^+_{j+3} + 37g^+_{j+4} + 2658g^+_{j-1} - 203g^+_{j-2}\Big) \\ &+ 9800\Big(g^+_j - \frac{328}{245}g^+_{j+1} + \frac{199}{245}g^+_{j+2} - \frac{8}{35}g^+_{j+3} + \frac{1}{35}g^+_{j+4} - \frac{64}{245}g^+_{j-1} - \frac{3}{245}g^+_{j-2}\Big)\xi \\ &+ 2760\Big(g^+_j + \frac{4}{69}g^+_{j+1} - \frac{17}{23}g^+_{j+2} + \frac{10}{23}g^+_{j+3} - \frac{5}{69}g^+_{j+4} - \frac{22}{23}g^+_{j-1} + \frac{19}{69}g^+_{j-2}\Big)\xi^2 \\ &- 5600\Big(g^+_j - \frac{8}{7}g^+_{j+1} + \frac{5}{7}g^+_{j+2} - \frac{8}{35}g^+_{j+3} + \frac{1}{35}g^+_{j+4} - \frac{16}{35}g^+_{j-1} + \frac{3}{35}g^+_{j-2}\Big)\xi^3 \\ &+ 1200\Big(g^+_j - \frac{4}{3}g^+_{j+1} + g^+_{j+2} - \frac{2}{5}g^+_{j+3} + \frac{1}{15}g^+_{j+4} - \frac{2}{5}g^+_{j-1} + \frac{1}{15}g^+_{j-2}\Big)\xi^4\ \Big], \end{aligned} \tag{2.9}$$

where $\xi = \frac{x-x_j}{\Delta x}$. We choose consecutive small stencils $S_l = [x_{j-r+l}, \ldots, x_{j+l+2}]$ for $l = 0, \ldots, r$, resulting in a series of lower order schemes.

In small stencil S_l, the polynomial $\rho_l(x)$ is satisfying:

$$\frac{1}{\Delta x^3}\int_{x_m-\frac{\Delta x}{2}}^{x_m+\frac{\Delta x}{2}}\int_{\eta-\frac{\Delta x}{2}}^{\eta+\frac{\Delta x}{2}}\int_{\xi-\frac{\Delta x}{2}}^{\xi+\frac{\Delta x}{2}}\rho_l(\theta)d\theta d\xi d\eta = g_m^+, \quad m = j-r+l, \ldots, j+l+2. \tag{2.10}$$

When $r = 2$, we can find three second degree polynomial expression which are based on nodal point information and satisfying the flux splinting:

$$\begin{aligned}
h_0(x) =& \frac{1}{\Delta x^2}\Big[\Big(\frac{3}{2}g_{j+1}^+ - \frac{1}{8}g_{j+2}^+ + \frac{3}{2}g_{j-1}^+ - \frac{1}{8}g_{j-2}^+ - \frac{11}{4}g_j^+\Big) - \Big(g_{j+1}^+ - \frac{1}{2}g_{j+2}^+ - g_{j-1}^+ + \frac{1}{2}g_{j-2}^+\Big)\xi \\
&+ (3g_j^+ - 2g_{j+1}^+ + \frac{1}{2}g_{j+2}^+ - 2g_{j-1}^+ + \frac{1}{2}g_{j-2}^+)\xi^2\Big], \\
h_1(x) =& \frac{1}{\Delta x^2}\Big[\Big(\frac{7}{8}g_{j-1}^+ - \frac{3}{2}g_j^+ + \frac{1}{4}g_{j+1}^+ + \frac{1}{2}g_{j+2}^+ - \frac{1}{8}g_{j+3}^+\Big) + \Big(5g_j^+ - 6g_{j+1}^+ + 3g_{j+2}^+ - \frac{1}{2}g_{j+3}^+ \\
&- \frac{3}{2}g_{j-1}^+\Big)\xi - \Big(2g_j^+ - 3g_{j+1}^+ + 2g_{j+2}^+ - \frac{1}{2}g_{j+3}^+ - \frac{1}{2}g_{j-1}^+\Big)\xi^2\Big], \\
h_2(x) =& \frac{1}{\Delta x^2}\Big[\Big(\frac{23}{8}g_j^+ - \frac{17}{2}g_{j+1}^+ + \frac{37}{4}g_{j+2}^+ - \frac{9}{2}g_{j+3}^+ + \frac{7}{8}g_{j+4}^+\Big) - \Big(\frac{5}{2}g_j^+ - 9g_{j+1}^+ + 12g_{j+2}^+ - 7g_{j+3}^+ \\
&+ \frac{3}{2}g_{j+4}^+\Big)\xi + \Big(\frac{1}{2}g_j^+ - 2g_{j+1}^+ + 3g_{j+2}^+ - 2g_{j+3}^+ + \frac{1}{2}g_{j+4}^+\Big)\xi^2\Big].
\end{aligned} \tag{2.11}$$

Step 2: We find the constant linear weights d_l, so that $h(x)$ on the big stencil is a linear combination of $h_l(x)$ on the small stencils with d_l as the combination coefficients

$$h(x_{j+\frac{1}{2}}) = \sum_{l=0}^{r} d_l h_l(x_{j+\frac{1}{2}}). \tag{2.12}$$

since by consistency $\sum_{l=0}^{r} d_l = 1$.

For the fifth-order approximation with three small stencils, from (2.12), we could obtain the linear weights

$$d_0 = \frac{4}{15}, \quad d_1 = \frac{1}{2}, \quad d_2 = \frac{7}{30}. \tag{2.13}$$

Step 3: We define the smoothness function, intending to maintain the same high order accuracy for smooth solutions and non-oscillatory performance near discontinuities of the scheme.

$$\beta_l = \sum_{\kappa=1}^{r}\Delta x^{2\kappa-1}\int_{I_j}\Big(\frac{d^\kappa}{dx^\kappa}h_l(x)\Big)^2 dx. \tag{2.14}$$

Its explicit expression for the case of $r = 2$ are:

$$\begin{aligned}
\beta_0 =& \frac{1}{3}\Big((3g_j^+ - 3g_{j+1}^+ + g_{j+2}^+ - g_{j-1}^+)^2 + (3g_j^+ - 3g_{j+1}^+ + g_{j+2}^+ - g_{j-1}^+)(g_{j+1}^+ - 3g_j^+ + 3g_{j-1}^+ - g_{j-2}^+) \\
&+ (-3g_j^+ + g_{j+1}^+ + 3g_{j-1}^+ - g_{j-2}^+)^2\Big) + (6g_j^+ - 4g_{j+1}^+ + g_{j+2}^+ - 4g_{j-1}^+ + g_{j-2}^+)^2, \\
\beta_1 =& \frac{1}{3}\Big((7g_j^+ - 9g_{j+1}^+ + 5g_{j+2}^+ - g_{j+3}^+ - 2g_{j-1}^+)^2 + (3g_j^+ - 3g_{j+1}^+ + g_{j+2}^+ - g_{j-1}^+)^2 \\
&+ (7g_j^+ - 9g_{j+1}^+ + 5g_{j+2}^+ - g_{j+3}^+ - 2g_{j-1}^+)(3g_j^+ - 3g_{j+1}^+ + g_{j+2}^+ - g_{j-1}^+)\Big) \\
&+ (4g_j^+ - 6g_{j+1}^+ + 4g_{j+2}^+ - g_{j+3}^+ - g_{j-1}^+)^2, \\
\beta_2 =& \frac{1}{3}\Big((-2g_j^+ + 7g_{j+1}^+ - 9g_{j+2}^+ + 5g_{j+3}^+ - g_{j+4}^+)^2 + (-3g_j^+ + 11g_{j+1}^+ - 15g_{j+2}^+ + 9g_{j+3}^+ - 2g_{j+4}^+)^2 \\
&+ (-2g_j^+ + 7\,g_{j+1}^+ - 9g\,{}_{j+2}^+ + 5g_{j+3}^+ - g_{j+4}^+)(-3g_j^+ + 11\,g_{j+1}^+ - 15g\,{}_{j+2}^+ + 9g_{j+3}^+ - 2g_{j+4}^+)\Big) \\
&+ (g_j^+ - 4g_{j+1}^+ + 6g_{j+2}^+ - 4g_{j+3}^+ + g_{j+4}^+)^2.
\end{aligned} \tag{2.15}$$

We expand the above smoothness indicators $\beta_l,\ l=0,1,2$ at grid point x_j:

$$\begin{aligned}
\beta_0 =&(g^+_{xxx})^2\Delta x^6+\Big(\frac{13}{12}(g^+_{xxxx})^2+\frac{1}{2}g^+_{xxx}g^+_{xxxxx}\Big)\Delta x^8+\Big(\frac{1}{16}(g^+_{xxxxx})^2+\frac{1}{20}g^+_{xxx}g^+_{xxxxxxx}\\
&+\frac{13}{36}g^+_{xxxx}g^+_{xxxxxx}\Big)\Delta x^{10}+O(\Delta x^{12}),\\
\beta_1 =&(g^+_{xxx})^2\Delta x^6+\Big(\frac{13}{12}(g^+_{xxxx})^2-\frac{1}{2}g^+_{xxx}g^+_{xxxxx}\Big)\Delta x^8+\Big(-\frac{1}{2}g^+_{xxx}g^+_{xxxxxx}+\frac{13}{60}g^+_{xxxx}g^+_{xxxxx}\Big)\Delta x^9\\
&+\Big(\frac{55}{48}(g^+_{xxxxx})^2-\frac{17}{60}g^+_{xxx}g^+_{xxxxxxx}+\frac{13}{9}g^+_{xxxx}g^+_{xxxxxx}\Big)\Delta x^{10}+O(\Delta x)^{11},\\
\beta_2 =&(g^+_{xxx})^2\Delta x^6+\Big(\frac{13}{12}(g^+_{xxxx})^2-\frac{7}{2}g^+_{xxx}g^+_{xxxxx}\Big)\Delta x^8+\Big(-5g^+_{xxx}g^+_{xxxxxx}+\frac{13}{3}g^+_{xxxx}g^+_{xxxxx}\Big)\Delta x^9\\
&+\Big(\frac{355}{48}(g^+_{xxxxx})^2-\frac{257}{60}g^+_{xxx}g^+_{xxxxxxx}+\frac{169}{36}g^+_{xxxx}g^+_{xxxxxx}\Big)\Delta x^{10}+O(\Delta x^{11}).
\end{aligned}\tag{2.16}$$

where the grid point subscript of all derivatives is ignored to avoid confusion. So we notice

$$\begin{aligned}
&\text{if}\ \ g^+_{xxx}\neq 0,\ \text{then}\ \beta_l=D(1+O(\Delta x^2))\ \text{for}\ l=0,1,2.\\
&\text{if}\ \ g^+_{xxx}=0, g^+_{xxxx}\neq 0,\ \text{then}\ \beta_l=D(1+O(\Delta x))\ \text{for}\ l=0,1,2.
\end{aligned}\tag{2.17}$$

In general, we have

$$\beta_l=D(1+O(\Delta x)).\tag{2.18}$$

Step 4: We change the linear weights d_l in (2.12) to nonlinear weights. We first consider the nonlinear weights in [11]:

$$\tilde{\omega}_l=\frac{d_l}{(\varepsilon+\beta_l)^2},\qquad\qquad \omega_l=\frac{\tilde{\omega}_l}{\sum\tilde{\omega}_l}.\tag{2.19}$$

Remark 1. By Taylor expansion, we notice in order to achieve the fifth-order accuracy for $r=2, l=0,\ldots,r$ in smooth region, it should at least satisfy $\omega_l-d_l=O(\Delta x^2)$.

However, if the nonlinear weights (2.19) are used, we can only achieve

$$\omega_l-d_l=O(\Delta x),\ \ l=0,\ldots,r.\tag{2.20}$$

with above smoothness indicators.

In order to increase the accuracy of the nonlinear weights, we choice to use the mapped WENO nonlinear weights introduced in [7]. Here the mapped weight function is defined:

$$\mathcal{G}_l(\omega)=\frac{\omega(d_l+d_l^2-3d_l\omega+\omega^2)}{d_l^2+\omega(1-2d_l)},\quad l=0,\ldots,r.\tag{2.21}$$

This function is a non-decreasing monotone function with the following properties:

$$\begin{aligned}
&1.\ 0\le\mathcal{G}_l(\omega)\le 1,\quad \mathcal{G}_l(0)=0,\ \ \mathcal{G}_l(1)=1.\\
&2.\ \mathcal{G}_l(\omega)\approx 0\ \text{if}\ \omega\approx 0,\quad \mathcal{G}_l(\omega)\approx 1\ \text{if}\ \omega\approx 1.\\
&3.\ \mathcal{G}_l(d_l)=\mathcal{G}_l'(d_l)=\mathcal{G}_l''(d_l)=0.\\
&4.\ \mathcal{G}_l(\omega)=d_l+O(\Delta x^6)\ \text{if}\ \omega=d_l+O(\Delta x^2).
\end{aligned}\tag{2.22}$$

The mapped nonlinear weights are then given by

$$\omega_l^M=\frac{\alpha_l^M}{\sum_{l=0}^2\alpha_l^M},\quad \alpha_l^M=\mathcal{G}_l(\omega_l),\quad l=0,\ldots,r.\tag{2.23}$$

Remark 2. By Taylor expansion of $\mathcal{G}_l(\omega_l)$ for d_l and with the condition (2.20), we have $\alpha_l^M = d_l + O(\Delta x^3)$. Finally, we obtain the expected order of accuracy $\omega_l^M = d_l + O(\Delta x^3), \quad l = 0, \ldots, r$.

Step 5: The final reconstruction of the semi-discrete finite difference mapped WENO flux is given by:

$$\hat{G}^+_{j+\frac{1}{2}} = \sum_{l=0}^{r} \omega_l^M h_l(x_{j+\frac{1}{2}}), \quad l = 0, \ldots, r. \tag{2.24}$$

If we use the linear weights and linear combination on the right-hand side of (2.12), then we would get back the linear scheme on the big stencil, which will be accurate for smooth solutions but will be oscillatory near discontinuities.

Remark 3. In later numerical experiment, we use the above fifth order direct WENO scheme ($r = 2$) for dispersion term in (1.1). For the first derivative, we use the fifth order finite difference WENO scheme with mapped nonlinear weights as (2.21), (2.23) and its corresponding linear weights in [7], so that we can achieve the fifth order computational accuracy in general.

Remark 4. The extension of present scheme to two-dimensional case, the spatial discretization procedure can be proceeded by dimensional by dimensional manner.

3. Runge–Kutta time discretization

Up until now we have considered only spatial discretization. Eq. (1.1) is equivalent to the first order ODE system after spatial discretization with finite difference WENO scheme [7] for first derivative and direct fifth-order WENO scheme obtained above for third derivative as:

$$\frac{du}{dt} = L(u). \tag{3.1}$$

This ODE system can be discretized by a suitable ODE solver. We use the third order total variation diminishing (TVD) Runge–Kutta method [6] to solve (3.1), which is given by

$$\begin{aligned} u^{(1)} &= u^n + \Delta t L(u^n), \\ u^{(2)} &= \frac{3}{4}u^n + \frac{1}{4}u^{(1)} + \frac{1}{4}\Delta t L(u^{(1)}), \\ u^{n+1} &= \frac{1}{3}u^n + \frac{2}{3}u^{(2)} + \frac{2}{3}\Delta t L(u^{(2)}). \end{aligned} \tag{3.2}$$

This explicit time discretization has the advantage of maintaining nonlinear stability. However, it may not be the most efficient solver because of the time step restriction $\Delta t = O(\Delta x^3)$. Nevertheless, for dispersion-dominated equations, this time discretization could still be a suitable choice.

In order to ensure numerical stability for dispersion term, the time step satisfying the Courant–Friedrich–Lewy (CFL) stability condition must be carefully selected. To determine the CFL condition of the form $\Delta t = CFL \cdot \Delta x^3$, we consider the fifth order finite difference scheme on big stencil and the third order TVD Runge–Kutta method in time for the dispersion equation $u_t + u_{xxx} = 0$. Evaluate the numerical flux at $x_{j+\frac{1}{2}}$ by (2.9):

$$h(x_{j+\frac{1}{2}}) = -\frac{1}{15}g^+_{j-2} + \frac{21}{40}g^+_{j-1} + \frac{1}{8}g^+_j - \frac{23}{12}g^+_{j+1} + \frac{7}{4}g^+_{j+2} - \frac{19}{40}g^+_{j+3} + \frac{7}{120}g^+_{j+4}. \tag{3.3}$$

The numerical flux at $x_{j-\frac{1}{2}}$ also can be obtained by simply shift (3.3) by one point to the left. Inserting these to (2.3) and applying the third order TVD Runge–Kutta method in time direction, we can deduce the amplification

Table 4.1
Order of accuracy at $T = \frac{1}{2}$ in $x \in [-10, 10]$ for Example 2.

N	L_∞	order	L_1	order	L_2	order
80	2.4085e−02		4.0875e−03		6.7210e−03	
160	1.0183e−03	4.5640	1.8039e−04	4.5020	2.9209e−04	4.5242
320	2.8075e−05	5.1807	5.2863e−06	5.0927	8.6104e−06	5.0842
640	8.4993e−07	5.0458	1.7414e−07	4.9239	2.7673e−07	4.9596

factor by Fourier transform:

$$\begin{aligned} Q(\zeta,\sigma) = 1 &- \sigma\Big(-\frac{71}{120}\big(\cos(\zeta)-i\sin(\zeta)\big)^2 - \frac{49}{15}\cos(\zeta) - \frac{61}{15}i\sin(\zeta) + \frac{49}{24} + \frac{89}{40}\big(\cos(\zeta)+i\sin(\zeta)\big)^2 \\ &- \frac{8}{15}\big(\cos(\zeta)+i\sin(\zeta)\big)^3 + \frac{7}{120}\big(\cos(\zeta)+i\sin(\zeta)\big)^4 + \frac{1}{15}\big(\cos(\zeta)-i\sin(\zeta)\big)^3\Big) \\ &+ \frac{1}{2}\sigma^2\Big(-\frac{71}{120}\big(\cos(\zeta)-i\sin(\zeta)\big)^2 - \frac{49}{15}\cos(\zeta) - \frac{61}{15}i\sin(\zeta) + \frac{49}{24} + \frac{89}{40}\big(\cos(\zeta)+i\sin(\zeta)\big)^2 \\ &- \frac{8}{15}\big(\cos(\zeta)+i\sin(\zeta)\big)^3 + \frac{7}{120}\big(\cos(\zeta)+i\sin(\zeta)\big)^4 + \frac{1}{15}\big(\cos(\zeta)-i\sin(\zeta)\big)^3\Big)^2 \\ &- \frac{1}{6}\sigma^3\Big(-\frac{71}{120}\big(\cos(\zeta)-i\sin(\zeta)\big)^2 - \frac{49}{15}\cos(\zeta) - \frac{61}{15}i\sin(\zeta) + \frac{49}{24} + \frac{89}{40}\big(\cos(\zeta)+i\sin(\zeta)\big)^2 \\ &- \frac{8}{15}\big(\cos(\zeta)+i\sin(\zeta)\big)^3 + \frac{7}{120}\big(\cos(\zeta)+i\sin(\zeta)\big)^4 + \frac{1}{15}\big(\cos(\zeta)-i\sin(\zeta)\big)^3\Big)^3. \end{aligned} \tag{3.4}$$

where $\sigma = \frac{\Delta t}{\Delta x^3}$. From the stability condition $|Q(\sigma,\zeta)| \le 1$ for all $\zeta \in [-\pi,\pi]$, we obtain the CFL condition

$$0 < \sigma = \frac{\Delta t}{\Delta x^3} \le 0.30480. \tag{3.5}$$

4. Numerical tests

In the following examples, we present numerical results and analysis for some dispersion-type equations with various initial conditions. Since the explicit third-order TVD Runge–Kutta method is applied for time direction, the CFL stability condition requires the step size on time direction as:

$$\Delta t \le \min\Big(\frac{CFL\cdot\Delta x^{\frac{5}{3}}}{\max(|f'(u)|)}, \frac{CFL\cdot\Delta x^3}{\max(|g'(u)|)}\Big). \tag{4.1}$$

For all numerical simulations in this paper, we take $CFL = 0.3$ as obtained by Fourier analysis for the linear dispersion equation in the previous section.

Example 1. We compute the classical soliton solution of the KdV equation in nonlinear case:

$$u_t - 3(u^2)_x + u_{xxx} = 0, \quad -10 \le x \le 10. \tag{4.2}$$

The exact solution is $u(x,t) = -2\mathrm{sech}^2(x-4t)$. The accuracy order is measured with periodic boundary condition and initial condition extracted from the exact solution. The numerical errors in terms of L_1, L_2 and L_∞ norms and fifth-order convergency order at $T = 1$ in $x \in [-10, 10]$ can be seen in Table 4.1.

Example 2. We compute the conservation law with zero dispersion limit

$$u_t + \Big(\frac{u^2}{2}\Big)_x + \varepsilon u_{xxx} = 0, \tag{4.3}$$

with continuous initial condition

$$u(x,0) = 2 + 0.5\sin(2\pi x), \quad 0 \le x \le 2\pi$$

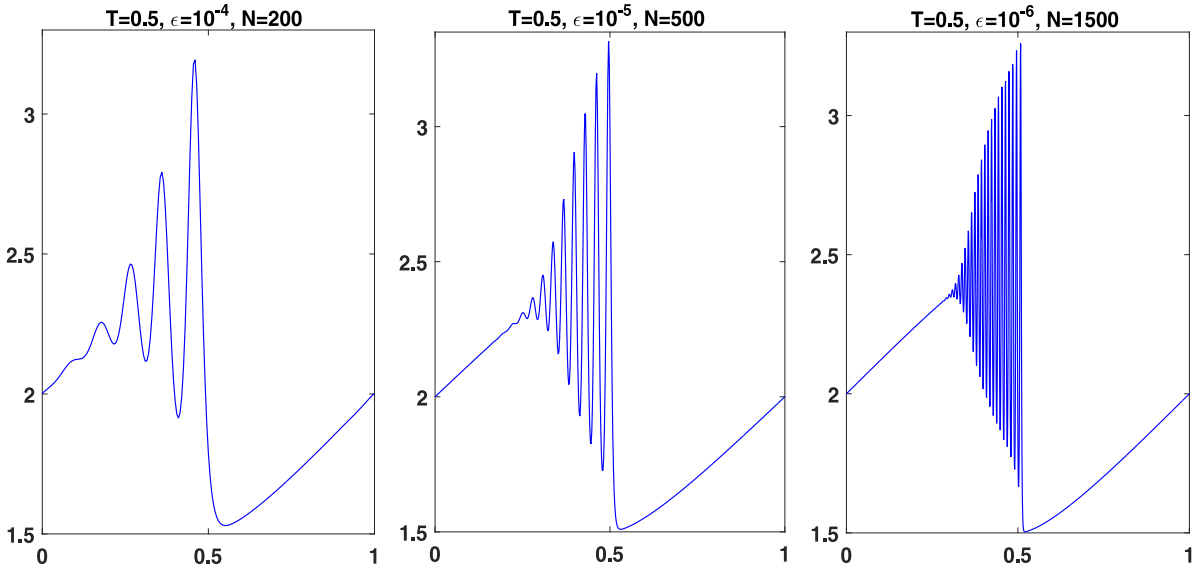

Fig. 4.1. Numerical solution of KdV equation with $T = 0.5$ in $x \in [0, 2\pi]$ for Example 2.

and discontinuous initial condition

$$u(x, 0) = \begin{cases} 1 & 0.25 < x < 4, \\ 0 & \text{else.} \end{cases}$$

Considering this dispersive nonlinear KdV equation($\varepsilon \to 0$) with periodic boundary condition, dispersive shock wave behavior is expected for small ε. In this example, we illustrate the capability of our code in resolving high-frequency wavelets for very small ε and produce continuous wavelets in the vicinity of the discontinuity. The solution is simulated at $T = 0.5$ with $\varepsilon = 10^{-4}, 10^{-5}, 10^{-6}$, respectively, and plotted in Fig. 4.1. For comparison, the similar physical downstream oscillations of the continuous wavelets are captured in [15,18]. The results show that the solutions are noise-free particularly before and after the dispersive shock.

Consider above equation with discontinuous initial condition and inflow–outflow boundary condition, we can observe a left-propagating dispersion-shock wave in every discontinuous interface and the amplitude of the wave increases through time. The evolution of a top-hat initial solution into a train of traveling waves can be observed from Fig. 4.2, which even with physical discontinuous initial data, the zero-dispersion limit solutions are not discontinuous, but evolve fine-scale continuous wavelets, eventually separating into solitary waves. The dispersion-shock wave in discontinuous interface plotted with present scheme seems to be more accurate and elastic than the ones plotted with [17,18] under the same mesh.

Example 3. In this example, we show the numerical simulations for the Ito-type coupled nonlinear problem

$$\begin{cases} u_t - (3u^2 + v^2)_x - u_{xxx} = 0, \\ v_t - 2(uv)_x = 0. \end{cases} \tag{4.4}$$

with initial condition

$$u(x, 0) = \cos(x), \quad v(x, 0) = \cos(x). \tag{4.5}$$

and Gaussian initial condition

$$u(x, 0) = \exp(-x^2), \quad v(x, 0) = \exp(-x^2). \tag{4.6}$$

with periodic boundary condition.

Dispersive wave and shock-similarity wave profile can be observed for u and v, respectively, from Figs. 4.3 and 4.4. These results are coincide with the ones obtained by Local discontinuous Galerkin method in [23].

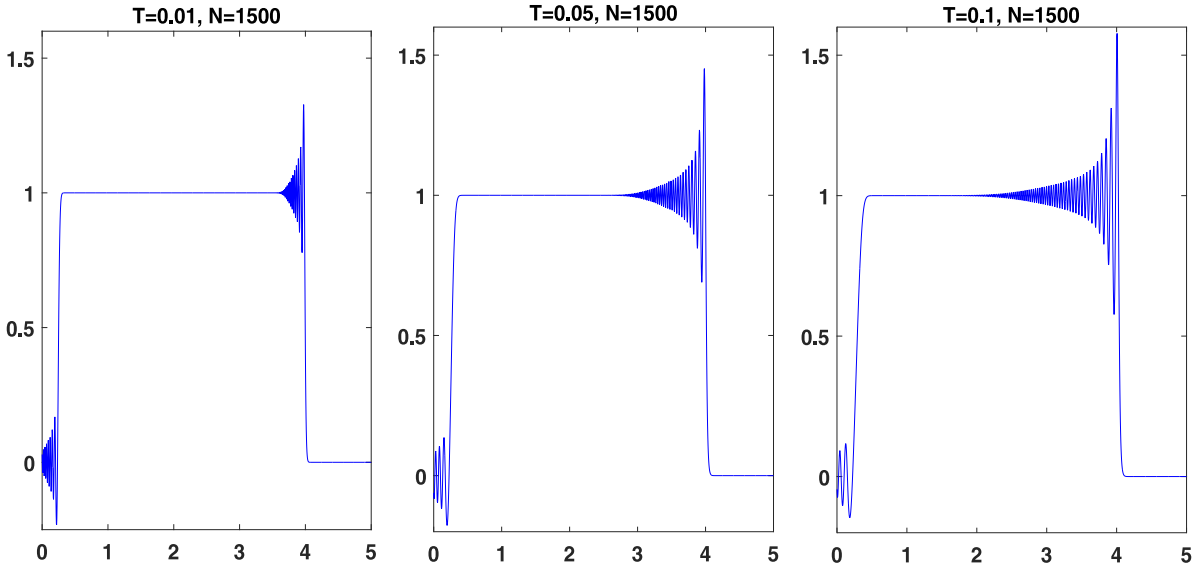

Fig. 4.2. Numerical solution of KdV equation with $\varepsilon = 10^{-4}$ at $T = 0, 0.01, 0.05, 0.1$ in $x \in [0, 5]$ for Example 2.

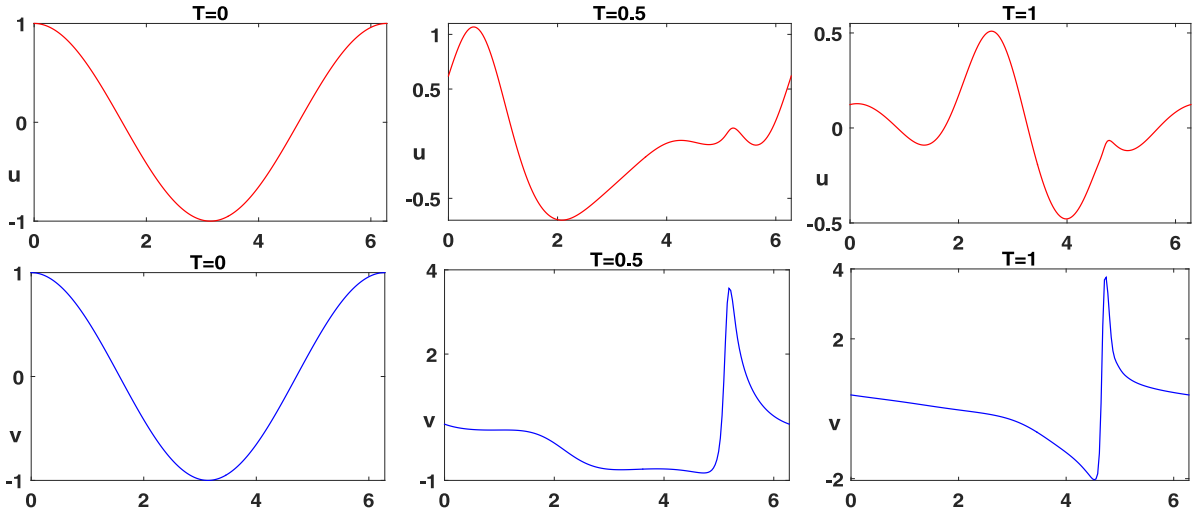

Fig. 4.3. Numerical solution of Ito's equation with 200 cells at $T = 0, 0.5, 1$ in $x \in [0, 2\pi]$ with periodic boundary condition and initial condition (4.5) for Example 3.

Example 4. Considering the nonlinear dispersive case, we simulate the $K(2, 2)$ equation

$$u_t + (u^2)_x + (u^2)_{xxx} = 0 \tag{4.7}$$

with the canonical traveling wave solution

$$u(x,t) = \begin{cases} \frac{4\lambda}{3}\left[\cos\left(\frac{x-\lambda t}{4}\right)\right]^2, & |x - \lambda t| \le 2\pi, \\ 0, \quad \text{Otherwise.} \end{cases} \tag{4.8}$$

In order to measure the accuracy of the scheme without the interference of the non-smooth interfaces, take the computational domain $[-2\pi, 2\pi]$ with periodic boundary condition for the solution (4.8). The fifth-order accuracy of the scheme is tested and listed in Table 4.2.

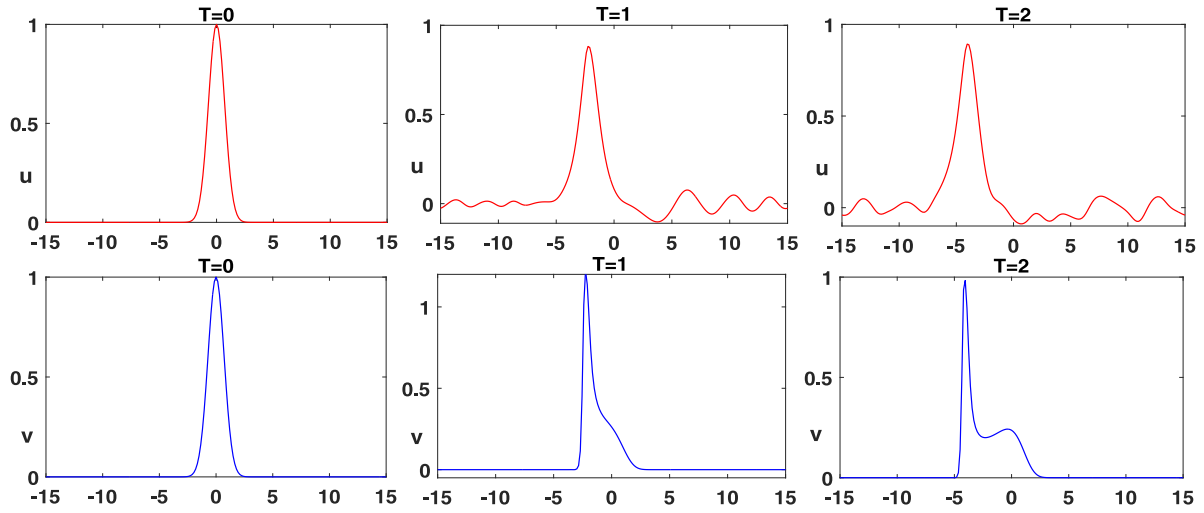

Fig. 4.4. Numerical solution of Ito's equation with 200 cells at $T = 0, 1, 2$ in $x \in [-15, 15]$ with periodic boundary condition and initial condition Eq. (4.6) for Example 3.

Table 4.2
Order of accuracy for $K(2,2)$ equation at $T = \frac{\pi}{2}$ in computational domain $x \in [-2\pi, 2\pi]$ with periodic boundary condition for Example 4.

N	L_∞	order	L_1	order	L_2	order
40	2.3296e−05		1.0091e−05		1.2034e−05	
80	1.7095e−07	7.0904	6.9898e−08	7.1736	8.0308e−08	7.2273
160	4.6023e−09	5.2150	2.0391e−09	5.0992	2.3109e−09	5.1190
320	1.2242e−10	5.2325	6.8360e−11	4.8986	7.6499e−11	4.9169

To observe compacton-splitting behavior of $K(2,2)$ equation, we take the initial data:

$$u_0(x) = \begin{cases} \frac{4}{3}\cos^2(\frac{x}{8}), & x \in [-4\pi, 4\pi], \\ 0 & \text{otherwise.} \end{cases} \tag{4.9}$$

The wave motion at $T = 10, 25, 50$ are simulated and displayed in Fig. 4.5 in domain $[-5\pi, 25\pi]$ with $N = 600$ cells. We can observe that the compactons split from one initial compacton as time evolves and move to the right. At the same time, a small residue is developed at the left interface, similarly to the LDG scheme [13]. It can be observed that no Gibbs oscillations develop in the non-smooth interface (the edges of the compactons). The small residue, which seems to be a compacton–anti-compacton pair, appeared in the left side of the compacton-packet seems to be a physical one, this also detected by the LDG scheme [13]. Our scheme can distinguish between numerical oscillation and physical oscillation without any other special treatment.

Example 5. Considering the $K(3,3)$ equation

$$u_t + (u^3)_x + (u^3)_{xxx} = 0. \tag{4.10}$$

We compute the compacton-collision behavior of $K(3,3)$ equation with the initial data:

$$u(x,0) = \begin{cases} \sqrt{3}\cos(\frac{x-10}{3}), & |x-10| \le \frac{3\pi}{2}, \\ \frac{3}{2}\cos(\frac{x-25}{3}), & |x-25| \le \frac{3\pi}{2}, \\ \sqrt{\frac{3}{2}}\cos(\frac{x-40}{3}), & |x-40| \le \frac{3\pi}{2}, \\ 0 & \text{otherwise.} \end{cases} \tag{4.11}$$

As can be seen in Fig. 4.6, three compactons with various speeds pass through with each other during nonlinear interaction while propagating to the right, and also maintain their coherent shapes after the collision. Despite the

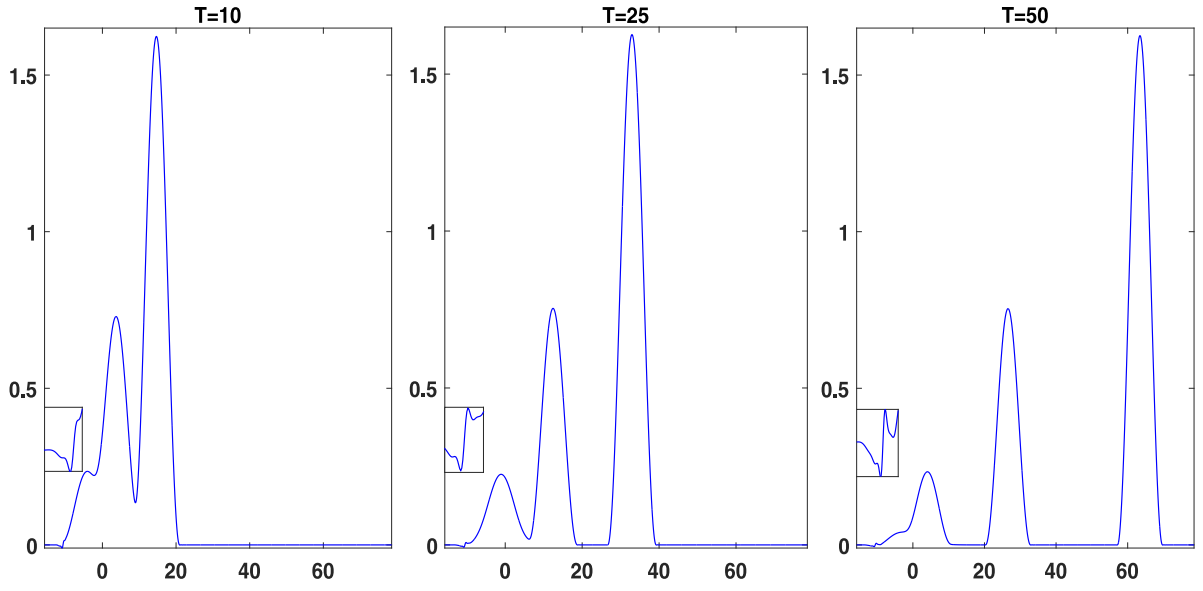

Fig. 4.5. Numerical solution of $K(2,2)$ equation with $N = 600$ at $T = 10, 25, 50$ in $x \in [-5\pi, 25\pi]$ for Example 4.

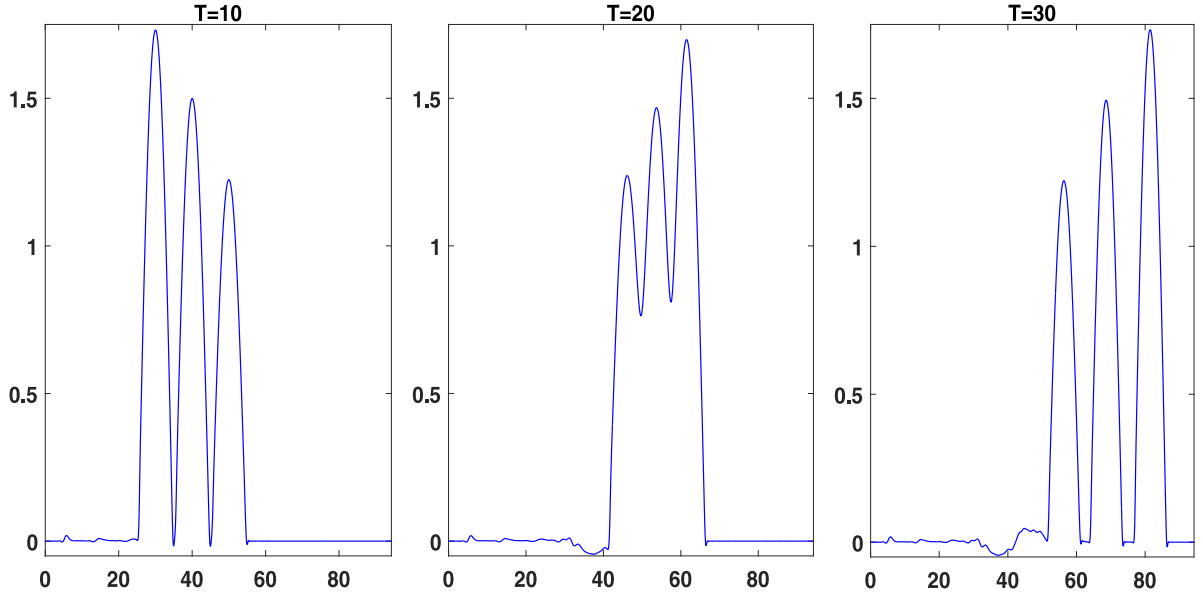

Fig. 4.6. Numerical solution of $K(3,3)$ with $N = 600$ at $T = 10, 20, 30$ in $x \in [0, 30\pi]$ for Example 5.

compactons emerge out intactly from the collision, a small residue is bounced back from the collision on the left. Similar results are also can be found in [13]. These compactons are found to be not fully elastic as mentioned in [19], and also obtained in the original compacton study [9]. The wavelets of the residue get even more clear along with mesh-refinement. According to earlier-published compacton studies and numerical observation, we believe that this phenomena is not numerically induced.

In order to observe the superiority of the direct WENO scheme over the same order finite difference scheme, we also compare the results of the WENO scheme with linear weights (finite difference method in big stencil) and WENO scheme with nonlinear weights in Fig. 4.7 for the compacton-collision case of $K(3,3)$ equation with initial

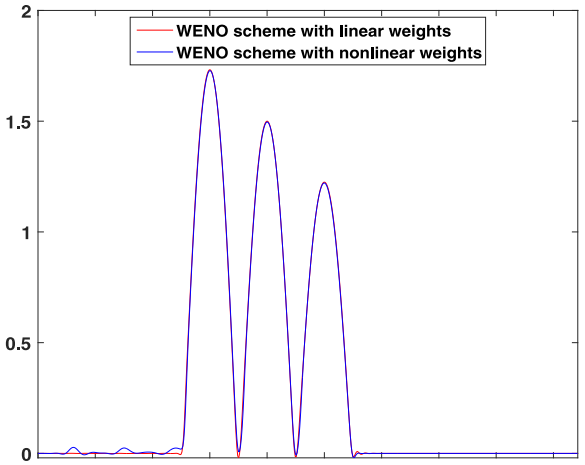

Fig. 4.7. Comparison of direct WENO scheme with linear weights and direct WENO scheme with nonlinear weights with $N = 600$ at $T = 10$ in $x \in [0, 30\pi]$ for Example 5.

Table 4.3
Order of accuracy for linear dispersion equation at $T = 1$ in computational domain $(0, 2\pi) \times (0, 2\pi)$ with periodic boundary condition for Example 6.

N	L_∞	order	L_1	order	L_2	order
10	8.4957e−03		5.1664e−03		5.9701e−03	
20	2.0644e−04	5.3629	1.2972e−04	5.3157	1.4522e−04	5.3615
40	5.6188e−06	5.1993	3.5778e−06	5.1802	3.9742e−06	5.1914
80	1.7408e−07	5.0124	1.1080e−07	5.0130	1.2310e−07	5.0127

data (4.11) under the coarse mesh. Obviously, the WENO scheme with nonlinear weights has the advantages of detecting this compacton residue while the WENO scheme with linear weights smoothes out completely.

Example 6. We consider two-dimensional linear dispersion equation:

$$u_t + u_{xxx} + u_{yyy} = 0. \tag{4.12}$$

The exact wave solution is of the form $u(x, y, t) = \sin(x + y + 2t)$. We can see in Table 4.3 that the method gives the fifth order of convergence with periodic boundary condition in domain $(0, 2\pi) \times (0, 2\pi)$. For two-dimensional problem, the computation is proceeded by dimension-by-dimension manner.

Example 7. Considering the compacton-splitting case of 2D-$K(2, 2)$ equation:

$$u_t + (u^2)_x + (u^2)_y + (u^2)_{xxx} + (u^2)_{yyy} = 0. \tag{4.13}$$

with initial date:

$$u(x, y, 0) = \begin{cases} 2\big(\operatorname{sech}(x + \lambda y - x_0)\big)^2, & |x + \lambda y - x_0| \le \pi, \\ 0, & \text{Otherwise.} \end{cases} \tag{4.14}$$

where $\lambda = 1, x_0 = 6$.

The numerical solutions of compacton-splitting case of $K(2, 2)$ equation obtained at the time level $T = 2, 4, 6, 10$ with number of grid number $N_x = N_y = 80$ are shown in Fig. 4.8. A similar wave residue with one-dimensional case still can be observed along with propagation.

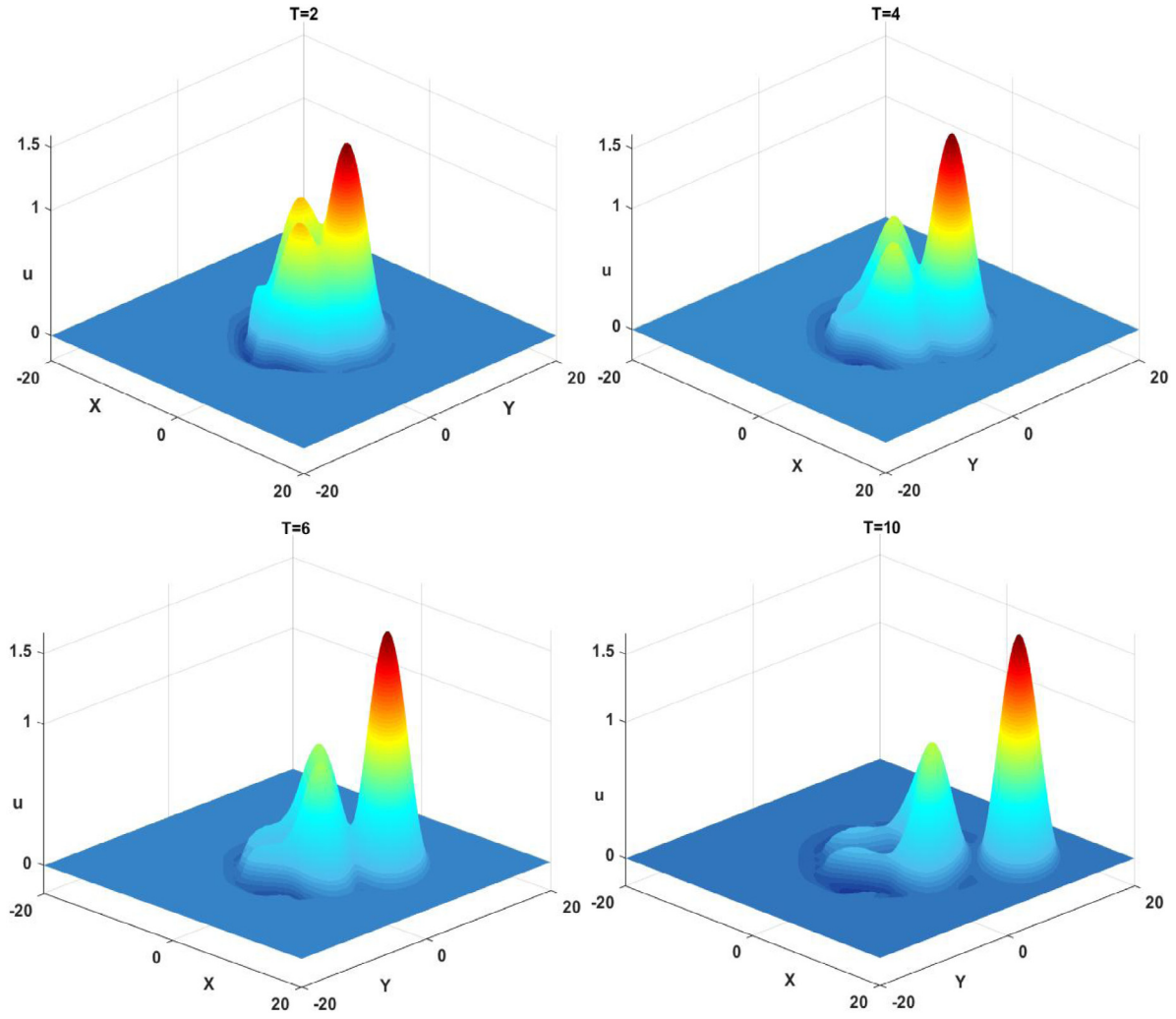

Fig. 4.8. Compacton-Splitting of $K(2,2)$ equation with $N_x = N_y = 80$ at $T = 2, 4, 6, 10$ in $[-20, 20] \times [-20, 20]$ for Example 7.

5. Concluding remark

We derive high order accurate direct weighted essentially non-oscillatory (WENO) scheme for the third derivative by direct approximation in this paper. Numerical tests are provided for the simulation of linear dispersion equation, KdV equation, Ito equation, $K(2,2)$ and $K(3,3)$ equation with various initial conditions. To our knowledge, dispersion-type equations may have smooth, high-frequency oscillation, peakon, or shock wave behavior depending on nonlinearity and smoothness. Here we observe the wave motion of some dispersion-type equations with smooth, discontinuous initial data obtained by our scheme at hand. Numerical results show that our present scheme is effective and has the advantages of high-order accuracy and non-oscillatory property. On the other hand, present scheme imposes damping on physical oscillations, and we assume that this is due to the flux treatment of the third derivative of the direct WENO scheme since we do not know the exact or entropy wave velocity in theory. Dissipation increases obviously with the increase of the nonlinearity degree on third derivative, and the current Lax–Friedrichs flux treatment is no longer sufficient. That is what we are going to focus on in the future.

CRediT authorship contribution statement

Muyassar Ahmat: Conceptualization, Methodology, Software, Writing – original draft. **Jianxian Qiu:** Conceptualization, Methodology, Supervision, Writing – review & editing.

References

[1] Rooholah Abedian, A new high-order weighted essentially non-oscillatory scheme for non-linear degenerate parabolic equations, Numer. Methods Partial Differ. Equ. 37 (2) (2021) 1317–1343.

[2] Rooholah Abedian, Hojatollah Adibi, Mehdi Dehghan, A high-order weighted essentially non-oscillatory (WENO) finite difference scheme for nonlinear degenerate parabolic equations, Comput. Phys. Commun. 184 (8) (2013) 1874–1888.

[3] Todd Arbogast, Chieh-Sen Huang, Xikai Zhao, Finite volume WENO schemes for nonlinear parabolic problems with degenerate diffusion on non-uniform meshes, J. Comput. Phys. 399 (2019) 108921.

[4] Dinshaw S Balsara, Chi-Wang Shu, Monotonicity preserving weighted essentially non-oscillatory schemes with increasingly high order of accuracy, J. Comput. Phys. 160 (2) (2000) 405–452.

[5] Alina Chertock, Doron Levy, Particle methods for dispersive equations, J. Comput. Phys. 171 (2) (2001) 708–730.

[6] Sigal Gottlieb, David I Ketcheson, Chi-Wang Shu, Strong Stability Preserving Runge-Kutta and Multistep Time Discretizations, World Scientific, 2011.

[7] Andrew K Henrick, Tariq D Aslam, Joseph M Powers, Mapped weighted essentially non-oscillatory schemes: Achieving optimal order near critical points, J. Comput. Phys. 207 (2) (2005) 542–567.

[8] X.Y. Hu, Q Wang, Nikolaus A Adams, An adaptive central-upwind weighted essentially non-oscillatory scheme, J. Comput. Phys. 229 (23) (2010) 8952–8965.

[9] M.S. Ismail, T.R. Taha, A numerical study of compactons, Math. Comput. Simul. 47 (6) (1998) 519–530.

[10] Yan Jiang, High order finite difference multi-resolution WENO method for nonlinear degenerate parabolic equations, J. Sci. Comput. 86 (1) (2021) 1–20.

[11] Guang-Shan Jiang, Chi-Wang Shu, Efficient implementation of weighted ENO schemes, J. Comput. Phys. 126 (1) (1996) 202–228.

[12] Doron Levy, Gabriella Puppo, Giovanni Russo, Compact central WENO schemes for multidimensional conservation laws, SIAM J. Sci. Comput. 22 (2) (2000) 656–672.

[13] Doron Levy, Chi-Wang Shu, Jue Yan, Local discontinuous Galerkin methods for nonlinear dispersive equations, J. Comput. Phys. 196 (2) (2004) 751–772.

[14] Xu-Dong Liu, Stanley Osher, Tony Chan, Weighted essentially non-oscillatory schemes, J. Comput. Phys. 115 (1) (1994) 200–212.

[15] Hongxia Liu, Jianxian Qiu, Finite difference Hermite WENO schemes for hyperbolic conservation laws, J. Sci. Comput. 63 (2) (2015) 548–572.

[16] Yuanyuan Liu, Chi-Wang Shu, Mengping Zhang, High order finite difference WENO schemes for nonlinear degenerate parabolic equations, SIAM J. Sci. Comput. 33 (2) (2011) 939–965.

[17] Alireza Mazaheri, Hiroaki Nishikawa, Very efficient high-order hyperbolic schemes for time-dependent advection–diffusion problems: Third-, fourth-, and sixth-order, Comput. Fluids 102 (2014) 131–147.

[18] Alireza Mazaheri, Mario Ricchiuto, Hiroaki Nishikawa, A first-order hyperbolic system approach for dispersion, J. Comput. Phys. 321 (Supplement C) (2016) 593–605.

[19] Bogdan Mihaila, Andres Cardenas, Fred Cooper, Avadh Saxena, Stability and dynamical properties of Rosenau-Hyman compactons using Padé approximants, Phys. Rev. E 81 (5) (2010) 056708.

[20] Samala Rathan, Rakesh Kumar, Ameya D Jagtap, L1-type smoothness indicators based WENO scheme for nonlinear degenerate parabolic equations, Appl. Math. Comput. 375 (2020) 125112.

[21] Philip Rosenau, James M Hyman, Compactons: Solitons with finite wavelength, Phys. Rev. Lett. 70 (5) (1993) 564.

[22] Philippe Saucez, A Vande Wouwer, W.E. Schiesser, P Zegeling, Method of lines study of nonlinear dispersive waves, J. Comput. Appl. Math. 168 (1–2) (2004) 413–423.

[23] Yan Xu, Chi-Wang Shu, Local discontinuous Galerkin methods for the Kuramoto–Sivashinsky equations and the Ito-type coupled KdV equations, Comput. Methods Appl. Mech. Eng. 195 (25–28) (2006) 3430–3447.

[24] Zhuang Zhao, Jun Zhu, Yibing Chen, Jianxian Qiu, A new hybrid WENO scheme for hyperbolic conservation laws, Comput. FLuids 179 (2019) 422–436.

[25] Jun Zhu, Jianxian Qiu, A new fifth order finite difference WENO scheme for solving hyperbolic conservation laws, J. Comput. Phys. 318 (2016) 110–121.